ELSEVIER

Journal of Photochemistry and Photobiology A: Chemistry 148 (2002) 57–64

Journal of Photochemistry and Photobiology A:Chemistry

www.elsevier.com/locate/jphotochem

Nanostructured ZnO electrodes for dye-sensitized solar cell applications

K. Keis [a], C. Bauer [a], G. Boschloo [a], A. Hagfeldt [a,*], K. Westermark [b], H. Rensmo [b], H. Siegbahn [b]

[a] *Department of Physical Chemistry, Uppsala University, P.O. Box 532, S-75121 Uppsala, Sweden*
[b] *Department of Physics, Uppsala University, P.O. Box 530, S-75121 Uppsala, Sweden*

Received 24 July 2001; received in revised form 1 October 2001; accepted 1 October 2001

Abstract

Dye-sensitized photoelectrochemical solar cells constitute a promising candidate in the search for cost-effective and environment-friendly solar cells. The most extensively studied, and to date the most efficient systems are based on titanium dioxide. In this paper, the possibilities to use nanostructured ZnO electrodes in photoelectrochemical solar cells are investigated. Various experimental techniques (e.g. infrared, photoelectron, femtosecond and nanosecond laser spectroscopies, laser flash induced photocurrent transient measurements, two- and three-electrode photoelectrochemical measurements) show that the thermodynamics, kinetics and charge transport properties are comparable for ZnO and TiO_2. The preparation techniques of ZnO provide more possibilities of varying the particle size and shape compared to TiO_2. However, the dye-sensitization process is more complex in case of ZnO and care needs to be taken to achieve an optimal performance of the solar cell.

Keywords: Zinc oxide; Nanostructured; Dye-adsorption; Solar cells

1. Introduction

Solar cells based on dye-sensitized nanostructured metal oxides are promising for low-cost solar energy conversion and are intensively investigated nowadays. Systems based on the *cis*-bis(isothiocyanato)bis(2,2′-bipyridyl-4,4′-dicarboxylato)-ruthenium(II) (or $Ru(dcbpyH_2)_2(NCS)_2$) sensitizer adsorbed onto nanostructured TiO_2 films are the most extensively studied and, at present, the most efficient for photoelectrochemical (PEC) solar cells [1,2]. One advantage with dye-sensitized PEC solar cells is the flexibility in the choice of material, in which all included components can be varied and their properties may be fine-tuned. This is especially true for nanostructured electrodes where beside the band gap, band gap position and surface structure, the particle size and shape, doping density, porosity, film thickness are important parameters to optimize.

Several attempts have been made to use ZnO in PEC solar cells. Dye-sensitized semiconducting single-crystal ZnO electrodes were studied by Gerischer and Tributsch [3,4] as early as 1969. In 1980, a 2.5% energy conversion efficiency at 562 nm using sintered porous disks of ZnO was reported by Matsumura et al. [5]. In the following years many different dyes were tried for the photosensitization of ZnO electrodes, e.g. chlorophyll [6], phthalocyanines [7], rhodamine B [8], coumarins [9], rose-bengal [5,10], Cu(I)- [11,12] and Ru(II)-complexes [13]. In 1994 Redmond et al. [14] achieved an incident photon-to-current conversion efficiency (IPCE) of 13% at 520 nm when using the $Ru(dcbpyH_2)_2(NCS)_2$ dye. In our laboratory, the initial tests of ZnO in PEC solar cells were promising: IPCE values of 50–60% at 540 nm and an overall solar energy conversion efficiency of 2% was obtained under 56 mW/cm^2 illumination with a solar simulator [15]. Recently, for the mercurochrome-sensitized ZnO PEC solar cell a solar energy conversion efficiency under 99 mW/cm^2 illumination reaching 2.5% has been reported [16]. However, the efficiency is still moderate compared to solar cells based on TiO_2.

In this paper, the possibility to use nanostructured ZnO electrodes in PEC solar cells is discussed. Summarizing the work performed in our laboratory as well as published in the literature by other researchers, a comparison between solar cells based on ZnO and TiO_2 is made and discussed in terms of energy level matching, light harvesting efficiency, charge carrier injection and electron transport properties.

* Corresponding author. Tel.: +46-18-471-3642; fax: +46-18-508-542.
E-mail address: anders.hagfeldt@fki.uu.se (A. Hagfeldt).

1010-6030/02/$ – see front matter
PII: S1010-6030(02)00039-4

The differences and similarities between the two materials are highlighted.

2. Preparation aspects

2.1. Preparation of ZnO particles

From a synthetic aspect, control of particle size, shape and composition by wet chemical methods is readily achieved when preparing ZnO particles, whereas several limitations are encountered in making TiO_2 [17]. ZnO particles with the wurtzite crystal structure have the advantage of being formed spontaneously even at low temperatures (0 °C). The preparation of ZnO particles with nanometer sizes based on sol–gel methods have been reported [18–21]. These nanometer sized particles are generally prepared in two steps. Firstly, an ethanolic solution of zinc acetate is heated in order to prepare an intermediate species through hydrolysis and condensation. Secondly, LiOH is added to induce further growth. From these colloids, nanostructured films are prepared by applying a colloidal ZnO solution onto a conducting glass substrate by spin coating or doctor blading. The films are then fired at temperatures around 400 °C.

Additionally, ZnO particles with various sizes, shapes and compositions have been precipitated by means of hydrolysis of zinc salts in the presence of different amines [22–26]. This method allows the synthesis of ZnO particles in aqueous solution at low temperatures (<100 °C). The reaction kinetics, nucleation and particle growth can be influenced by experimental parameters such as pH, precursor type, concentration, stoichiometry, temperature and time of aging. After precipitation of the ZnO powder, nanostructured film electrodes can be prepared by several methods. In our laboratory we have used two different methods. In the first, dispersions are made by grinding the prepared powder with acetylacetone and water with a subsequent addition of a small amount of Triton X-100 [15,26]. In this case the films are made by doctor blading using a glass rod and adhesive tape spacers, followed by a sintering step. In the second method, the colloidal solution is obtained by mixing ZnO powder with ethanol. The suspensions are applied onto the substrate by doctor blading followed by compression of the deposited particle layer onto the conducting substrate at room temperature under 1000 kg/cm^2 pressure [27]. This new method for manufacturing nanostructured electrodes is described in detail elsewhere [28,29]. The firing step is not necessary in this case since no organic additives are present in the film and the electrical contact between particles is achieved by the compression. A scanning electron microscope picture of a ZnO electrode prepared in this way is shown in Fig. 1.

2.2. Dye-sensitization of ZnO

Dye-sensitization is achieved by immersing the nanostructured electrode into a 0.5 mM ethanolic dye solution. Carboxyl groups are commonly used anchoring groups for chemisorption of dye molecules onto metal oxide surfaces [2]. For TiO_2, the strong adsorption of the carboxyl groups to the surface favors monolayer growth. For ZnO, on the other hand, the sensitization process is more complex. For the frequently used dyes, such as *cis*-bis(isothiocyanato)bis(2,2′-bipyridyl-4,4′-dicarboxylato)-ruthenium(II) (or $Ru(dcbpyH_2)_2(NCS)_2$) and *cis*-bis(isothiocyanato)bis(2,

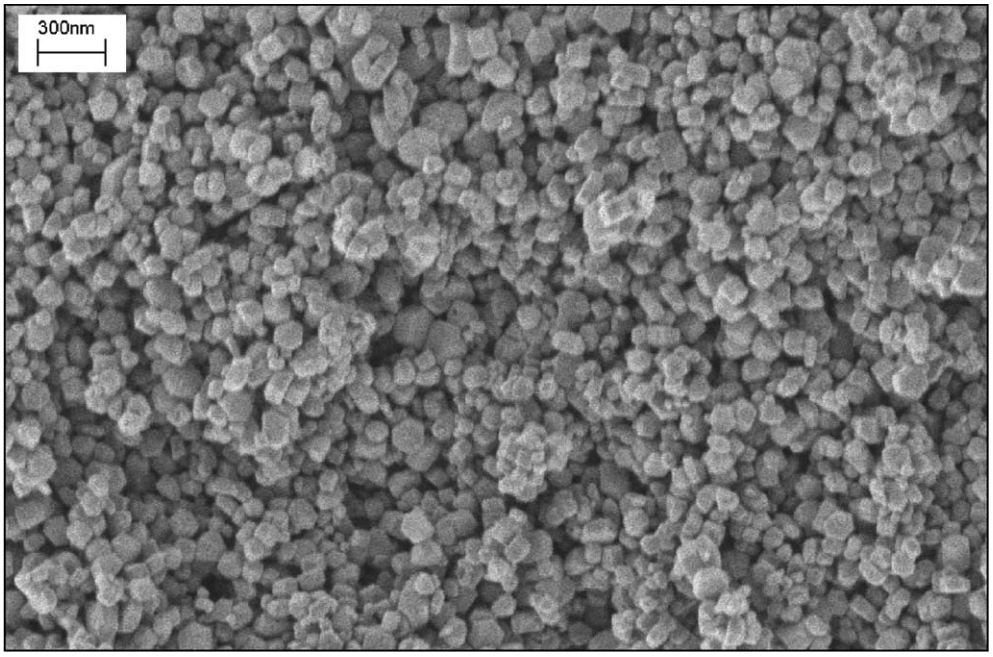

Fig. 1. SEM picture of a nanostructured ZnO electrode prepared by the compression method. The average particle size is 150 nm.

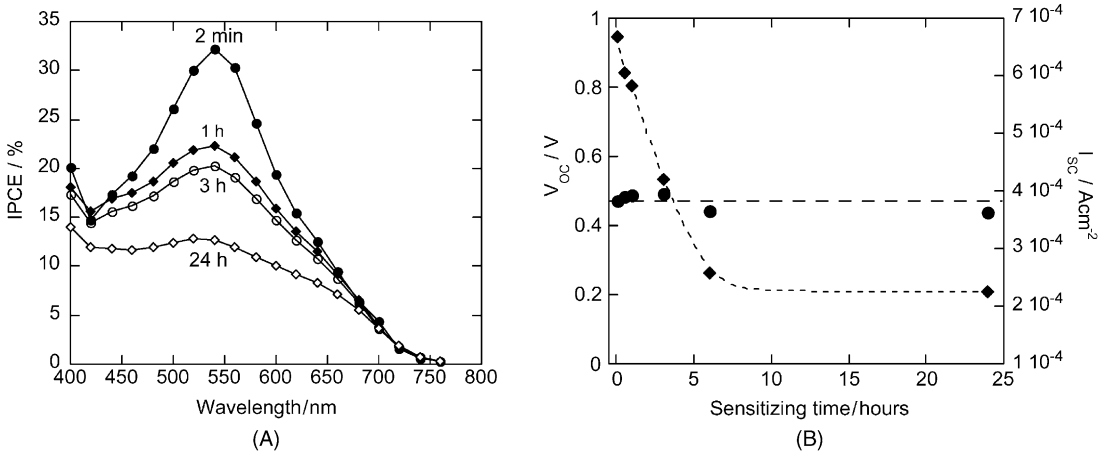

Fig. 2. The effect of the sensitizing time in 0.5 mM Ru[dcbpy(TBA)$_2$]$_2$(NCS)$_2$ on (A) the IPCE action spectra and (B) the short circuit current density (diamonds) and open circuit voltage (spheres) under 60 W/m^2 illumination. The ZnO films used were 10 μm thick based on 150 nm sized particles. The electrolyte solution used was 0.5 M LiI/50 mM I_2 in 3-methoxypropionitrile.

2′-bipyridyl-4,4′-dicarboxylato)-ruthenium(II) bis-tetrabutylammounium (or Ru[dcbpy(TBA)$_2$]$_2$(NCS)$_2$), sensitization of ZnO may be described by the following processes: diffusion of the dye into the ZnO nanostructure, adsorption of the dye to the ZnO surface, dissolution of Zn surface atoms from ZnO and formation of Zn^{2+}/dye complexes in the pores of the ZnO film [30]. Depending on the rate of these different processes, the outer part of the electrode may be in the process of forming Zn^{2+}/dye complexes in the pores when dye molecules reach the interface between the back-contact and the ZnO film. Thus, the latter process is on the way to increasing the efficiency, whereas the former is in the phase of decreasing the efficiency. The results in Fig. 2 are consistent with such processes. The IPCE decreases with longer times in the dye solution as well as the short circuit current (I_{SC}). The results indicate that protons from dyes cause the dissolution of Zn surface atoms and the formation of Zn^{2+}/dye complexes in the pores of the nanostructured film, which gives rise to a filter effect (inactive dye molecules). Consequently, the net yield for charge carrier injection is decreased whereas the light harvesting efficiency is increased due to the large number of dye molecules in the film, as discussed below. The complex formation between Zn^{2+}-ions originating from ZnO surface and different sensitizers is reported in the literature [31,32]. The formation of metal-ion/dye complexes does not take place in the case of TiO_2 electrodes but is apparently extremely important in case of ZnO. Based on these facts, careful control of the dye composition, concentration, pH and sensitization time is necessary in order to avoid the Zn^{2+}/dye complex formation and to achieve high efficiency solar cells based on ZnO.

One possible reason why protons from the carboxyl groups of the dye initiate a dissolution process of the ZnO and a formation of Zn^{2+}/dye complexes is related to the surface properties of the oxide. The point of zero charge (pzc) of metal oxides is defined as the pH where the concentrations of protonated and deprotonated surface groups are equal. It means that the surface is predominantly positively charged at pH below pzc and negatively charged above this value. The pH for the dye-sensitization process (pH = 5) is much lower than the pH of pzc of ZnO ($pH_{pzc} \approx 9$). Bahnemann [21] has shown that dissolution of ZnO colloids occur below pH 7.4. Thus, the protons adsorbed on the ZnO surface will dissolve the ZnO. In the case of TiO_2 the pH of the dye solution is similar to the pzc of the oxide. Another difference between TiO_2 and ZnO relates to the fact that Ti atoms are predominately 6-fold coordinated in the bulk whereas the Zn atoms are 4-fold coordinated. Thus, the typical surface coordinations of 5 and 3 for TiO_2 and ZnO, respectively, result in a relatively larger loss of coordination for ZnO. Moreover, theoretical investigations indicate that the bond length between Zn and O atoms on the ZnO $(1\,0\,\bar{1}\,0)$ surface increases upon the adsorption of formic acid, making the Zn–O bond weaker and prone to a Zn atom dissolution process [33].

3. Bonding geometry

Understanding of the interaction between the anchoring group of the dye molecule and the semiconductor surface is important in order to improve the photoelectrochemical performance of the solar cell. Information of the interaction may be obtained from IR spectral data (Fig. 3) by comparing the splitting of antisymmetric and symmetric carboxylate stretching bands of the adsorbed species with carboxylate ions in solution [34]. In the IR spectra of the ZnO–Ru(dcbpy-H_2)$_2$(NCS)$_2$ and ZnO–Ru[dcbpy(TBA)$_2$]$_2$(NCS)$_2$ systems, the spacing between the carboxylate stretching bands were 228 and 248 cm^{-1}, respectively. The results are similar to those measured on a TiO_2 system, indicating a similar bonding on these two materials [35,36]. However, photoelectron spectroscopic measurements of carboxylated ruthenium

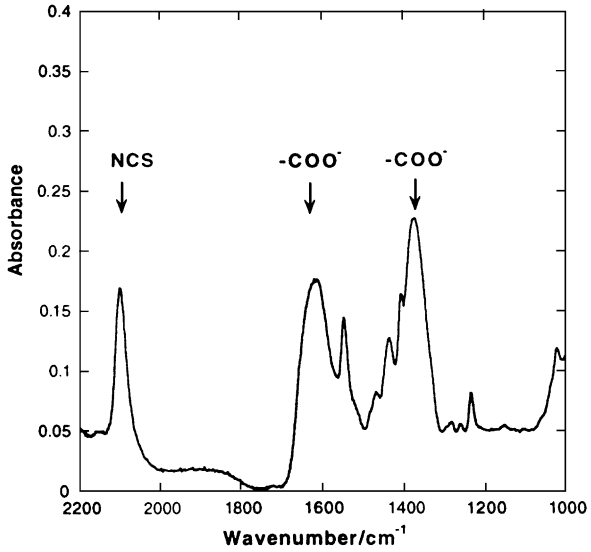

Fig. 3. The IR spectrum of a ZnO film dye-sensitized for 3 h in 0.5 mM $Ru[dcbpy(TBA)_2]_2(NCS)_2$.

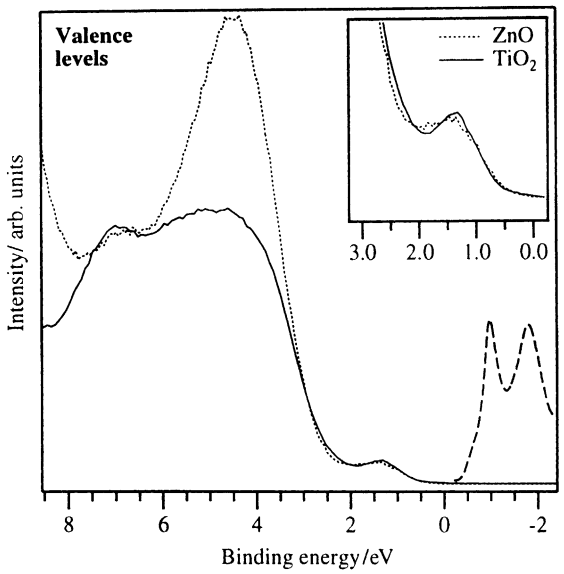

Fig. 4. Valence PES spectra of $Ru[dcbpyH_2]_2(NCS)_2$ adsorbed on TiO_2 (solid lines) and ZnO (dotted lines), energy calibrated with respect to the bipyridine N 1s level. The spectra were recorded at the Swedish National Synchrotron Source MAX, using a photon energy of 150 eV. The HOMO level of the dye is clearly distinguished above the valence band edge. The excited states of the dye (dashed lines) are positioned relative to the HOMO maximum for the dye adsorbed on TiO_2 [46].

complexes adsorbed onto nanostructured ZnO and TiO_2 indicate a bridge bonding (the carboxyl group is deprotonated and each oxygen atom interacts with a separate surface metal atom) in the case of TiO_2, whereas the carboxyl group was found to be protonated when binding to ZnO [37,38]. Adsorption on oxide surfaces has also been addressed by computational methods. Quantum chemical calculations have mostly been limited to small adsorbates such as formic acid on different ZnO surfaces and have been performed by several authors [39–44]. Theoretical studies of the adsorption of formic acid (HCOOH) on a ZnO $(1\,0\,\bar{1}\,0)$ surface energetically favor a bridging structure, which is also found to be the most stable adsorption mode [39,40]. However, the results also indicate that the bonding mode of formic acid on ZnO $(1\,0\,\bar{1}\,0)$ is sensitive to the surface coverage [40,45]. In addition, the adsorption is a dynamic process allowing translational mobility of the adsorbate on the surface. It is therefore likely that several bonding modes may be involved in the adsorbate interaction with ZnO surface.

4. Energetics

The energy level matching between dye and semiconductor is crucial for the performance of a solar cell. The injection efficiency of an electron from the dye to the semiconductor depends on the matching of the excited states of the dye molecule with the conduction band states. This matching is, in turn, related to the positions of the semiconductor valence band edge and the highest occupied molecular orbital (HOMO) level of the dye via the semiconductor band gap energy and the optical transition energies of the dye. The position of the HOMO level relative to the valence band can be measured by means of photoelectron spectroscopy (PES). This has been done earlier for different ruthenium complexes adsorbed on nanostructured TiO_2 [37]. Recently, the energy level matching for $Ru(dcbpyH_2)_2(NCS)_2$ adsorbed on nanostructured ZnO was compared with that of the same complex adsorbed on TiO_2 [46,47]. In Fig. 4, the valence PES spectra of this ruthenium complex adsorbed on TiO_2 and ZnO are shown. The dye HOMO level is clearly distinguished above the valence band edge for both semiconductors. The energy position of this peak with respect to the valence band of the semiconductor is similar in both cases. Since the bandgap is 3.2 eV for both zinc oxide and titanium dioxide, this result indicates that the energy matching between the dye and the metal oxide is similar for ZnO and TiO_2.

5. Electron injection and recombination kinetics

For the TiO_2–$Ru(dcbpyH_2)_2(NCS)_2$ system, the net yield for charge carrier injection is normally observed to be unity with electron injection occurring on a <100 fs time scale [48–51]. Redmond et al. [14] explained the low efficiencies for the ZnO–$Ru(dcbpyH_2)_2(NCS)_2$ system by the adsorption of dye molecules in such a manner that they do not efficiently inject an electron into the semiconductor upon photoexcitation. Studies of electron injection dynamics in dye-sensitized ZnO films by Asbury et al. [52] showed the presence of multiexponential injection kinetics with relatively slow injection times (ps), thus being different from TiO_2. However,

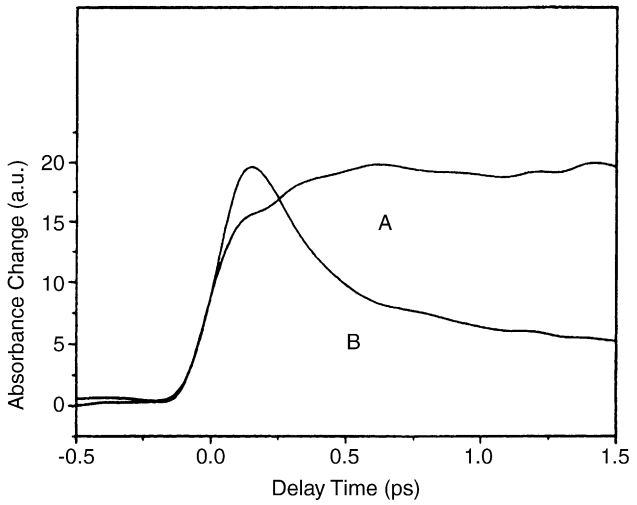

Fig. 5. Femtosecond pump-probe spectroscopy for studying electron injection dynamics. Transient absorption data collected with pump and probe wavelengths of 538 and 770 nm, respectively. (A) The ZnO–Ru[dcbpy(TBA)$_2$]$_2$(NCS)$_2$ system. The ZnO particles in this study were 15 nm sized and prepared by a sol–gel method [53]. The signal reflects the formation of the oxidized dye. (B) Bare Fe_2O_3 film. The signal reflects the immediate creation of electron–hole pair, and gives the rise time of the femtosecond laser system.

the high absorbance reported by Asbury et al. suggest that the Zn^{2+}/dye complex precipitation has occurred in the nanostructured film leading to the slow injection speed. Recently, the dynamics of electron transfer processes between Ru[dcbpy(TBA)$_2$]$_2$(NCS)$_2$ and nanostructured ZnO electrodes based on 15 nm sized particles were investigated in our group by femtosecond spectroscopy (Fig. 5). Under optimal preparation conditions, i.e. avoiding formation of dye-complexes in the pores of the ZnO film, the electron injection is ultrafast (<300 fs) [53]. Additionally, an estimation of the injection time from an analytical expression based on molecular and semiconductor parameters has been reported [54]. It predicts an increased injection time in the femtosecond domain for ZnO compared to TiO_2. However, the injection time is still sufficiently fast to make an efficient solar cell based on ZnO.

Besides the injection kinetics, electron transfer kinetics between conduction band electrons with oxidized dye and with tri-iodide present in the electrolyte solution need to be considered. For the TiO_2 system, the latter process occurs on a time scale of millisecond to second, and the recombination of injected electrons with oxidized dye occurs via surface states on a microsecond to millisecond time scale. Nanosecond laser flash photolysis studies of ZnO–Ru[dcbpy(TBA)$_2$]$_2$(NCS)$_2$ and TiO_2–Ru[dcbpy(TBA)$_2$]$_2$ (NCS)$_2$ systems, with similar particle size and number of dye molecules per semiconductor particle, indicate identical kinetics of back electron transfer for the two oxide systems, see Fig. 6 [53]. This result is surprising as the electronic structures of ZnO and TiO_2 conduction bands are essentially different.

6. Electron transport properties

The electron transport properties are influenced by the material morphology and its history (preparation method, synthesis conditions, etc.). By illuminating electrodes of different thicknesses, porosities, particle sizes and shapes with monochromatic light from different directions, information about the charge transport properties at low light intensities has been analyzed in our laboratory [26]. The electron transport in bare ZnO films is discussed below.

Nanoporous films based on 150 nm sized spherical ZnO particles (note: one order of magnitude larger than normally used in these systems) demonstrated good electron transport properties: high photoconversion efficiencies obtained from three-electrode measurements indicate low recombination

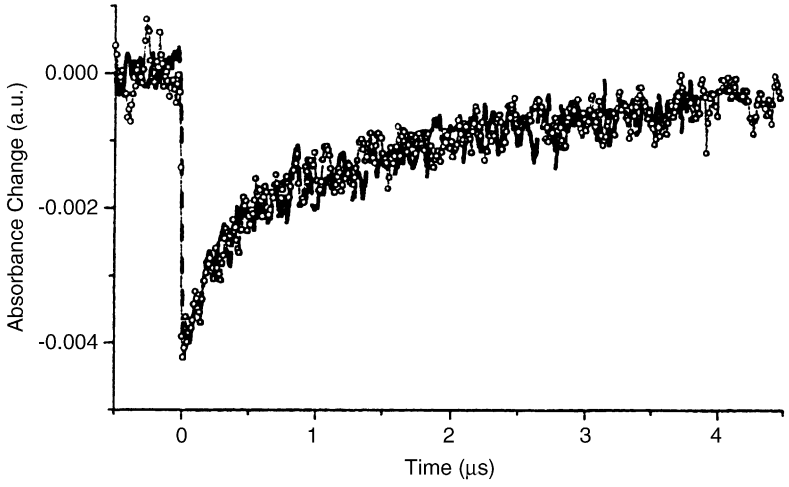

Fig. 6. Flash photolysis experiments performed for comparison of the recombination dynamics for ZnO (open circles) and TiO_2 (solid line). The electrodes were sensitized with Ru[dcbpy(TBA)$_2$]$_2$(NCS)$_2$. The traces show the recovery of the ground state (540 nm) after excitation at 510 nm.

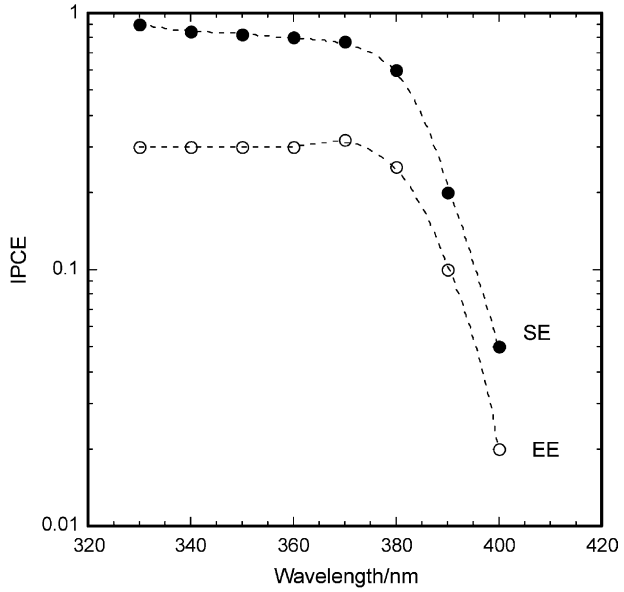

Fig. 7. Photocurrent action spectra for SE (substrate side) and EE (electrolyte side) illumination of a bare 8 μm thick ZnO electrode consisting of 150 nm sized spherical particles measured using a conventional three-electrode system enclosed in a Teflon vessel with quartz window. The electrolyte was 0.1 M KI in water, applied potential 300 mV vs. Ag/AgCl in saturated KCl.

losses during the transport (Fig. 7). In addition, electron losses to electron scavenging species in the electrolyte, such as oxygen and tri-iodide, were too small to be observed (Fig. 8). For nanostructured TiO_2 films it is known that the IPCE values decrease upon addition of electron scavengers to the electrolyte, i.e. a loss of electrons from the conduction band to tri-iodide or oxygen in the electrolyte [55]. There can be several reasons for not observing this effect in our ZnO studies. For 150 nm sized particles a band bending may be present. Additionally, the effective surface area is rather low which contributes to a general lowering of interfacial effects of electron-accepting species. However, steady-state results from a three-electrode measurement on smaller, 15 nm sized ZnO particles indicate that ZnO is still less sensitive to electron acceptors in the electrolyte than TiO_2. From electronic configurations the reactions with oxidizing species are expected only where the surface has been made oxygen deficient or bulk reduced. The crucial difference between the two materials is the existence of a stable lower oxidation state in TiO_2 (Ti^{3+}), leading to local electronic states in the bandgap. In ZnO this is not likely. Thus, the removal of electrons from cations in ZnO requires more energy than from reduced surface cations in TiO_2. Ultraviolet photoelectron spectroscopy (UPS) measurements indicate the depopulation of the Ti^{3+} defect states after exposure to O_2 [56]. Since the electron transfer rate is proportional to the number of available states at the surface, one could conclude either the presence of a larger number of surface states in TiO_2 compared to ZnO, or different energy distribution of such states in the bandgap. Laser flash induced photocurrent transient measurements indicate the same behavior: For a similar particle size of ZnO and TiO_2 (15 nm), the total charge collected for the thinnest (5 μm) and the thickest (24 μm) TiO_2 films differs by more than a factor of two, whereas for ZnO electrodes the difference is smaller [57]. This means that only a minor part of electron losses for ZnO occur during transport. In conclusion, the efficiency of collecting charge at the back-contact of nanostructured ZnO is equal to or higher than in TiO_2.

7. Summary

The electron transport properties of ZnO are similar to those of TiO_2. The light harvesting efficiency can also be made as efficient as TiO_2, but care must be taken in the

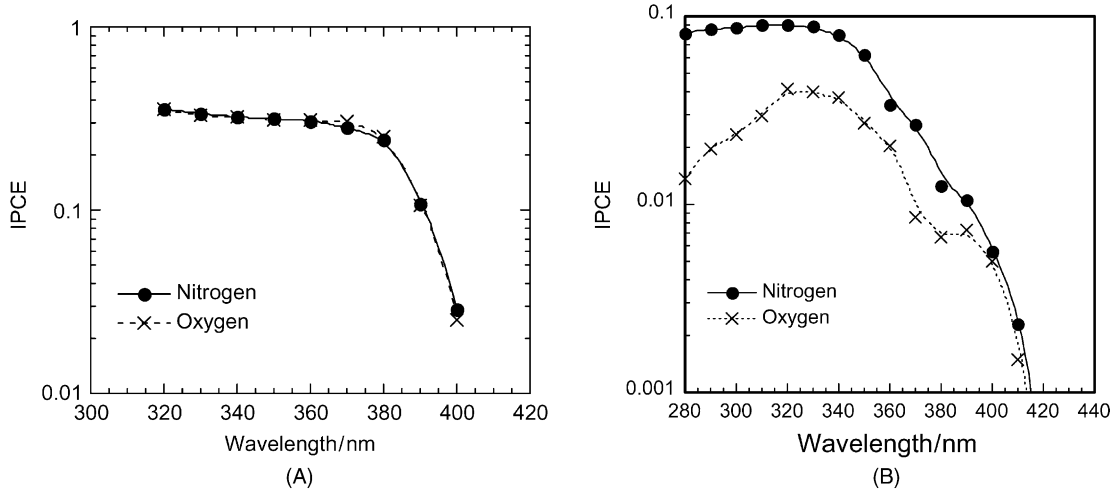

Fig. 8. Photocurrent action spectra (EE illumination) in nitrogen and oxygen atmospheres for bare (A) 30 μm thick ZnO film, consisting of 150 nm spherical particles [26]; (B) bare 8 μm thick TiO_2 film, consisting of 22 and 35 nm sized spherical particles, prepared from commercial TiO_2 (Degussa P25) powder [55]. In logarithmic scale. The measurements conditions are the same as in Fig. 7.

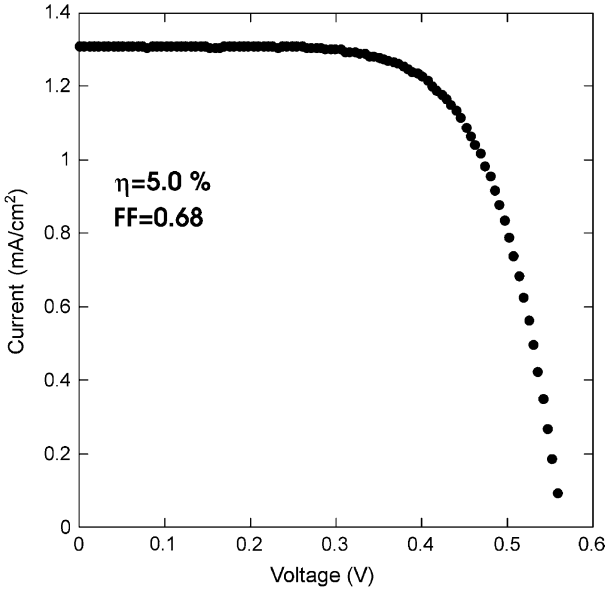

Fig. 9. *I–V* characteristics for 14 μm thick ZnO electrode (0.42 cm^2) sensitized in 0.5 mM $Ru[dcbpy(TBA)_2]_2(NCS)_2$ solution for 30 min. Illumination intensity 100 W/m^2. The electrolyte solution was 0.5 M LiI/50 mM I_2 and 0.5 M 4-tertbutylpyridine in 3-methoxypropionitrile.

dye-sensitization process. Under optimal dye-sensitization conditions, the electron injection rate for ZnO is slightly slower than for TiO_2, but still lies in the femtosecond domain. In our laboratory we have recently obtained a high overall efficiency of 5% of $Ru[dcbpy(TBA)_2]_2(NCS)_2$-sensitized ZnO solar cell (Fig. 9). This originates from a controlled dye-sensitization procedure (avoiding Zn^{2+}/dye complex formation) and from the new compression method (the exclusion of organic additives in preparation leading to better interfacial kinetics). This is close to the efficiencies we normally obtain with TiO_2 electrodes (∼6%) using similar techniques.

References

[1] B. O'Regan, M. Grätzel, Nature 353 (1991) 737.
[2] M.K. Nazeeruddin, A. Kay, I. Rodicio, R. Humphey-Baker, E. Myller, P. Liska, N. Vlachopoulos, M. Grätzel, J. Am. Chem. Soc. 115 (1993) 6382.
[3] H. Gerischer, H. Tributsch, Ber. Bunsenges. Phys. Chem. 73 (1969) 251.
[4] H. Gerischer, H. Tributsch, Ber. Bunsenges. Phys. Chem. 73 (1969) 850.
[5] M. Matsumura, S. Matsudaira, H. Tsubomura, Ind. Eng. Chem. Prod. Res. Dev. 19 (1980) 415.
[6] T. Miyasaka, T. Watanabe, A. Fujishima, K. Honda, J. Am. Chem. Soc. 100 (1978) 6657.
[7] N. Minami, T. Watanabe, A. Fujishima, K. Honda, Ber. Bunsenges. Phys. Chem. 83 (1979) 476.
[8] N. Alonso-Vante, V.M. Beley, P. Chartier, V. Ern, Rev. Phys. Appl. 16 (1981) 5.
[9] K. Murakoshi, S. Yanagida, M. Capel, E.W. Castner, Nanostructured Materials, Interfacial Electron Transfer Dynamics of Photosensitized Zinc Oxide Nanoclusters, Am. Chem. Soc. Publishers, 1997.
[10] H. Kokado, T. Nayama, E. Inoue, J. Phys. Chem. Solids 35 (1974) 1169.
[11] N. Alonso-Vante, J.F. Nierengarten, J.P. Sauvage, J. Chem. Soc., Dalton Trans. (1994) 1649.
[12] N. Alonso-Vante, V. Ern, P. Chartier, Nouveau J. Chem. 7 (1983) 3.
[13] I. Bedja, P. Kamat, X. Hua, G. Lappin, S. Hotchandani, Langmuir 13 (1997) 2398.
[14] G. Redmond, D. Fitzmaurize, M. Grätzel, Chem. Mater. 6 (1994) 686.
[15] H. Rensmo, K. Keis, H. Lindström, S. Södergren, A. Solbrand, A. Hagfeldt, S.-E. Lindquist, J. Phys. Chem. B 101 (1997) 2598.
[16] K. Hara, T. Horiguchi, T. Kinoshita, K. Sayama, H. Sugihara, H. Arakawa, Sol. Energy Mater. Sol. Cells 64 (2000) 115.
[17] Z.W. Wang, Characterization of Nanophase Materials, Wiley/VCH, Weinheim, 2000.
[18] M. Haase, H. Weller, A. Henglein, J. Phys. Chem. 92 (1988) 482.
[19] E.A. Meulenkamp, J. Phys. Chem. B 102 (1998) 2826.
[20] L. Spanhel, M.A. Anderson, J. Am. Chem. Soc. 113 (1991) 2826.
[21] D.W. Bahnemann, Israel J. Chem. 33 (1993) 115.
[22] M. Andes-Verges, A. Mifsud, C.J. Serna, J. Chem. Soc., Faraday Trans. 86 (1990) 959.
[23] M. Castellano, E. Matijevic, Chem. Mater. 1 (1989) 78.
[24] E. Matijevic, Langmuir 2 (1986) 12.
[25] M. Costa, J.L. Bapista, J. Eur. Ceram. Soc. 11 (1993) 275.
[26] K. Keis, L. Vayssieres, H. Rensmo, S.-E. Lindquist, A. Hagfeldt, J. Electrochem. Soc. 148 (2001) A149.
[27] K. Keis, E. Magnusson, H. Lindström, S.-E. Lindquist, A. Hagfeldt, Solar energy materials and solar cells 73 (1) (2002) 51–58.
[28] H. Lindström, A. Holmberg, E. Magnusson, S.-E. Lindquist, L. Malmqvist, A. Hagfeldt, Nanoletters 1 (2001) 97.
[29] H. Lindström, E. Magnusson, A. Holmberg, S.-E. Lindquist, A. Hagfeldt, Sol. Energy Mater. Sol. Cells, in press.
[30] K. Keis, J. Lindgren, S.-E. Lindquist, A. Hagfeldt, Langmuir 16 (2000) 4688.
[31] R. Baumeler, P. Rys, H. Zollingen, Helv. Chim. Acta 56 (1973) 2451.
[32] R. Brändli, P. Rys, H. Zollingen, H. Oswald, F. Schweizer, Helv. Chim. Acta 53 (1970) 1133.
[33] P. Persson, L. Ojamäe, Department of Quantum Chemistry, Uppsala University, Personal communication, 2000.
[34] K. Nakamoto, Infrared and Raman Spectra, Wiley, New York, 1986.
[35] N.W. Duffy, K.D. Dobson, K.C. Gordon, B.H. Robinson, A.J. McQuillan, Chem. Phys. Lett. 266 (1997) 451.
[36] K.S. Fillie, J.R. Barlett, J.L. Woolfrey, Langmuir 14 (1998) 2744.
[37] H. Rensmo, K. Westermark, S. Södergren, O. Kohle, P. Persson, S. Lunell, H. Siegbahn, J. Chem. Phys. 111 (1999) 2744.
[38] K. Westermark, H. Rensmo, A.C. Lees, J.G. Vos, H. Siegbahn, in preparation.
[39] H. Nakatsuji, M. Yoshimoto, Y. Umemura, S. Takagi, M. Hada, J. Phys. Chem. 100 (1996) 694.
[40] P. Persson, L. Ojamäe, Chem. Phys. Lett. 321 (2000) 302.
[41] S. Crook, H. Dhariwal, G. Thornton, Surf. Sci. 382 (1997) 19.
[42] W.T. Petrie, J.M. Vohs, Surf. Sci. 245 (1991) 315.
[43] R. Davis, J.F. Walsh, C.A. Muryn, G. Thornton, V.R. Dhanak, K.C. Prince, Surf. Sci. Lett. 298 (1993) L196.
[44] M. Yoshimoto, S. Takagi, Y. Umemura, M. Hada, H. Nakatsuji, J. Catal. 173 (1998) 53.
[45] P. Persson, Quantum photoelectrochemistry, theoretical studies of organic adsorbates on metal oxide surfaces, Acta Univ. Ups. Comprehensive Summaries of Uppsala Dissertations from the Faculty of Science and Technology, Vol. 544, 2000.
[46] K. Westermark, Dye/semiconductor interfaces, an electron spectroscopic study of systems for solar cell and display applications, Acta Univ. Ups. Comprehensive Summaries of Uppsala Dissertations from the Faculty of Science and Technology, Vol. 639, 2001.

[47] K. Westermark, H. Rensmo, H. Siegbahn, K. Keis, A. Hagfeldt, L. Ojamäe, P. Persson, in preparation.
[48] R.J. Ellingson, J.B. Asbury, S. Ferrere, H.N. Ghosh, T. Lian, A.J. Nozik, J. Phys. Chem. B 102 (1998) 6455.
[49] Y. Tachibana, J.E. Moser, M. Grätzel, D.R. Klug, J.R. Durrant, J. Phys. Chem. 100 (1996) 20056.
[50] T. Hannappel, B. Burfeindt, W. Storck, F. Willig, J. Phys. Chem. B 101 (1997) 6799.
[51] T. Heimer, E.J. Heilweil, J. Phys. Chem. B 101 (1997) 10990.
[52] J.B. Asbury, Y.Q. Wang, T. Lian, J. Phys. Chem. B 103 (1999) 6643.
[53] C. Bauer, G. Boschloo, E. Mukhtar, A. Hagfeldt, J. Phys. Chem. B 105 (2001) 5585.
[54] Å. Pettersson, M. Ratner, H.O. Karlsson, J. Phys. Chem. B 104 (2000) 8498.
[55] H. Rensmo, H. Lindström, S. Södergren, A.K. Willstedt, A. Solbrand, A. Hagfeldt, S.-E. Lindquist, J. Electrochem. Soc. 143 (1996) 3173.
[56] V.E. Heinrich, G. Dresselhaus, H.J. Zeiger, J. Vac. Sci. Technol. 15 (1978) 534.
[57] A. Solbrand, K. Keis, S. Södergren, H. Lindström, A. Hagfeldt, S.-E. Lindquist, Sol. Energy Mater. Sol. Cells 60 (2000) 181.